Supplementary Information

Two-Step Yielding in Jammed Microgel Suspension

Fayis Kanheerampockil[a,b,c], Rachna Maria Kurian[a], Gary Bryant[c]*, Suresh Bhat[a,b]*

[a] Polymer Science and Engineering DivisionCSIR-National Chemical Laboratory, Pune, Maharashtra 411008, India

[b] Academy of Scientific and Innovative Research (AcSIR) Ghaziabad, 201002, India

[c] Department of Physics, School of Science, RMIT University, Melbourne, VIC 3001, Australia

Corresponding Author

Email address: sk.bhat@ncl.res.in, gary.bryant@rmit.edu.au

I. Synthesis of core-shell microgels

Purified reactants, N-isopropylacrylamide (NIPAM) monomer and N,N'-methylenebisacrylamide (BIS) cross-linker, were mixed in 33 mL of deoxygenated deionized (DI) water. Sodium dodecyl sulfate (SDS, surfactant) and potassium peroxodisulfate (APS, initiator) were separately dissolved in 7 mL and 10 mL of DI water respectively. A 250 mL volume of DI water was added to the reaction vessel, and the temperature was maintained at 80°C. The monomer solution was initially added to the reaction medium at 80°C. After thorough mixing of the reactants, the SDS solution was introduced. Approximately two minutes later, the initiator APS solution was added to the reaction mixture. The initiation of polymerization was indicated by the transition from a transparent solution to a white, turbid appearance. The reaction was continued under stirring for 3 hours at 80°C to ensure complete conversion. Following this, the temperature was reduced to room temperature, and the microgels were stirred at 100 rpm overnight.

Table S1: Material details for the synthesis of core-shell microgels

Sample	NIPAM (g)	BIS (g)	SDS (g)	KPS (g)
N2.5	4.3	0.117	0.08	0.082
N20	4.3	0.937	0.08	0.082

II. Synthesis of homogeneously crosslinked microgel using continuous feed method

Homogeneously crosslinked microgels were synthesized following the method reported by Robert Acciaro[1]. Inhomogeneous crosslinking in microgels synthesized via the traditional batch synthesis process is attributed to the faster reactivity of the crosslinker relative to the NIPAm monomer. The crosslinker exhibits faster reaction rate, leading to the formation of a densely crosslinked core. As the concentration of the crosslinker decreases over time due to its faster reaction rate, a loosely crosslinked outer shell forms around the core. To counterbalance the impact of these differing reaction rates, Acciaro's article used a two-step feed synthesis approach. In the first step, calculated ratio of NIPAm-to-crosslinker was mixed, leading to the formation of seed particles. The reaction rate of NIPAm and the crosslinker was calculated to determine a specific NIPAm-to-crosslinker ratio for achieving the desired crosslink density in the seed particles. For instance, a ratio of 50 was optimized to achieve 5% crosslinked particles. In the second step, monomers were continuously added via a syringe pump at a flow rate of 200 mL/min. To maintain a constant monomer concentration and ensure uniform crosslink density of 5%, a monomer-to-crosslinker ratio of 20 was supplied through the feeding solution. Specific

amounts of the reactants, as shown in Table S2, were used to achieve 5% crosslinked particles. These amounts were determined by following the procedure and calculations reported by Acciaro et al.

In a typical reaction procedure, 0.43g of NIPAm monomer and 0.011g of BIS crosslinker were dissolved in 18 mL of Milli-Q water that had been pre-purged with Argon gas. This mixture was then transferred into the reactor, where the temperature was adjusted to 80 °C and the stirring speed was set to 300 rpm. Following the addition of the monomers into the reactor, 0.08g of SDS dissolved in 1 mL Milli-Q water was injected. One minute later, 1 mL of APS solution (APS~0.044g) was introduced in to the reaction mixture. The appearance of a light blue color indicated the initiation of the reaction. One minute after initiating the polymerization, the feeding solution containing NIPAm and BIS monomers was continuously fed into the reaction mixture. Typically, 4.409 g of NIPAm and 0.220 g of BIS were dissolved in 28.6 ml of water. The solution was degassed, loaded into a 60 mL syringe, and continuously fed into the reaction mixture at 200 µL/min using a syringe pump (Harvard Apparatus PHD2000). The feeding process continued for 143 minutes, and the reaction was then quenched by immersing the reactor in ice, reducing the temperature from 80°C to 15°C.

Table S2: Material details for the synthesis of homogeneous microgel particles using the continuous feed method.

Sample	NIPAM(g)		BIS(g)		SDS(g)		APS(g)	
	Reactor	**Feed**	**Reactor**	**Feed**	**Reactor**	**Feed**	**Reactor**	**Feed**
NH5	0.43	4.409	0.011	0.220	0.08	--	0.044	--

III. Dynamic Light scattering (DLS)

3D-dynamic light scattering (3D-DLS) was employed to determine the particle size over a range of scattering angles, θ, from 35° to 120°. The corresponding scattering vector is defined as $q = (4\pi n/\lambda) \times sin(\theta/2)$, where n is the refractive index of the solvent, λ is the wavelength of the incident laser. The measured intensity autocorrelation functions, $g^2(\tau) - 1$, were fitted using a single-exponential decay function of the form $A \times e^{(-2\Gamma\tau)}$, where Γ is the decay rate, τ is the delay time, and A is the intercept. The decay rates obtained at different angles were used to calculate the diffusion coefficient, D, via the relation $D = \frac{\Gamma}{q^2}$. The hydrodynamic radius, R_h, was

then determined using the Stokes-Einstein equation, $R_h = \frac{k_b T}{6\pi\eta D}$. Recorded $g^2(\tau) - 1$ data are shown in **Fig. S1**, and the corresponding R_h values are summarized in **Table S3**. For all samples, the standard deviation in R_h across the measured angular range is below 5%, indicating a high degree of monodispersity.

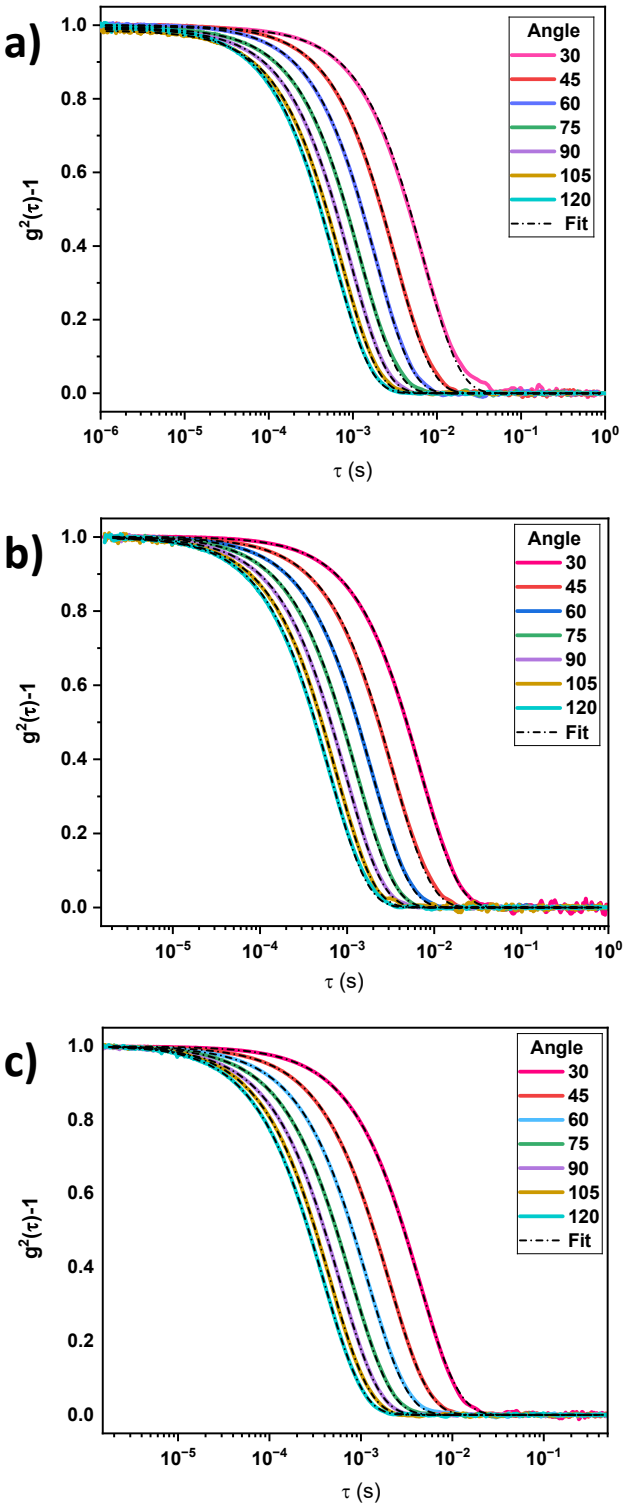

Fig. S1 Intensity auto correlation function v/s delay time, a) N2.5, b) NH5, and c) N20 particles. Dotted lines are the fits with single-exponential decay function of the form $A \times e^{(-2\Gamma\tau)}$.

Table. S3, the hydrodynamic diameter D_h, obtained from dynamic light scattering experiments for N2.5, NH5, N20 microgel particles.

Angle/D_h(nm)	N2.5	NH5	N20
30°	238	241	148
45°	241	254	152
60°	240	248	152
75°	236	243	150
90°	237	243	150
105°	234	241	149
120°	232	242	149

IV. Optical Properties.

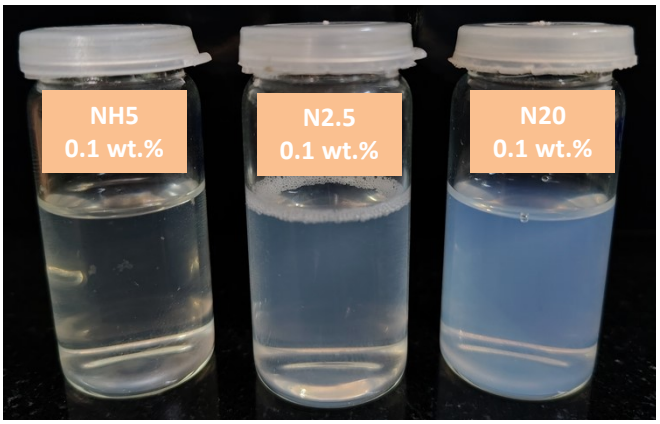

Fig.S2 Optical appearance of NH5, N2.5, N20 particles at 0.1 wt.%

V. Viscometry

Relative viscosity for N2.5, N20, and NH5 particles are plotted against the concentration in **Fig. S2**. The conversion factor k is determined by fitting with **Eq. 1** in the main text. The k values for N2.5, N20, and NH5 microgels are 0.136, 0.085, and 0.19, respectively. k values are used to convert c(wt %) to the volume fraction (ϕ) by the equation $\phi = kc$.

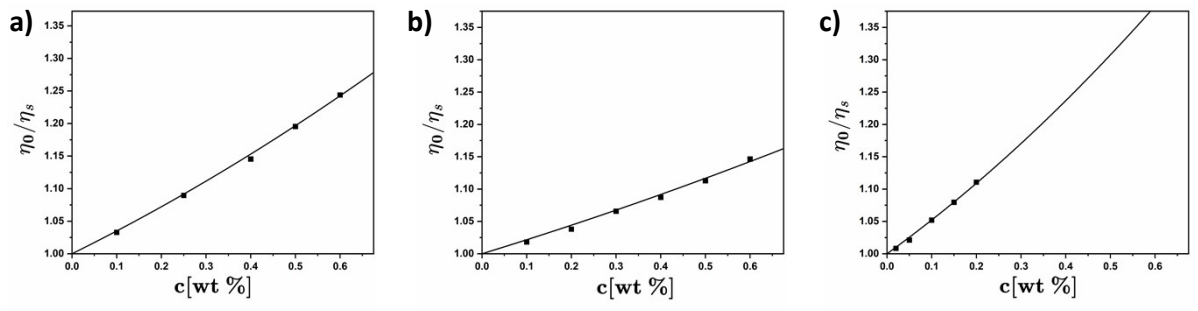

Fig. S3. Relative viscosity, η_o/η_s, versus concentration, c (wt %), for microgels: (a) core-shell 2.5% crosslinked microgels (N2.5), (b) core-shell 20% crosslinked microgels (N20), and (c) homogeneous 5% crosslinked microgels (NH5). Solid lines: fits by **Eq. 1** in the main text.

VI. Flow curves for jammed glass regime.

The criterion $\frac{\sigma_y R_h^3}{k_B T} \ll 12.5$, which defines the glassy regime as reported by Ikeda and coworkers[2], is used to distinguish the entropic glass from the jammed glass regimes. Using this criterion, **Fig. S3** shows that the jamming concentration for the N20 particle suspension occurs at $\phi_{eff} \approx 1.82$, while for the NH5 particles, it occurs at $\phi_{eff} \approx 5.97$. For the N2.5 particles, σ_y=39.2 for $\phi_{eff} \approx 3.52$ (Table. T1), resulting in $\frac{\sigma_y R_h^3}{k_B T} = 16.61$. This value confirms that the N2.5 particles, with $\phi_{eff} \geq 3.52$, lie within the jammed glassy regime.

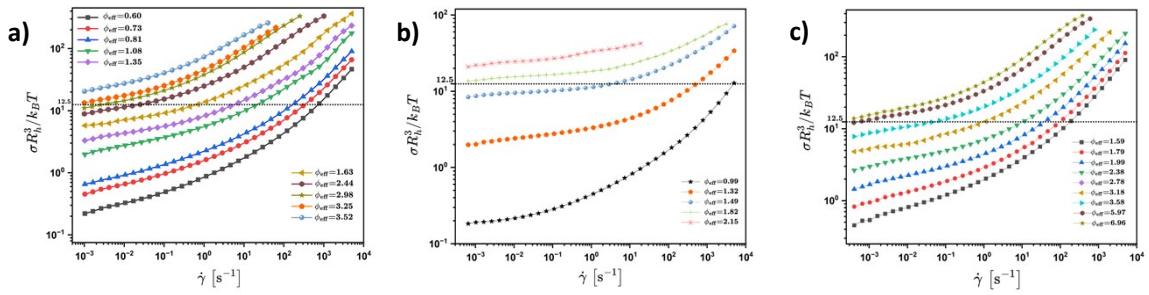

Fig. S4. Normalized shear stress, $\sigma R_h^3/k_B T$, versus shear rate, $\dot{\gamma}$, a) N2.5 microgels for various concentrations. (b), N20 microgels for various concentrations. (c), NH5 microgels for various concentrations. $\frac{\sigma_y R_h^3}{k_B T} = 12.5$, marking the boundary between the jammed (> 12.5) and entropic glass (< 12.5) regimes.

VII. Dynamic strain sweep experiments and Jamming volume fraction.

Fig. S5 a, b shows the dynamic strain sweep experiments conducted on N20 and NH5 particles at various volume fractions. **Fig. S5 c** shows the strain at which G'' attains its maximum, $\gamma_{G'' Peak}$, obtained from strain sweep experiments, plotted as a function of effective volume fraction. In **Fig. S5c** termination of the intermediate plateau region is identified as the jamming point, highlighted by green spheres in the plot. The corresponding jamming volume fractions are ϕ_{eff} = 2.71, 2.18, 4.75 for N2.5, N20, and NH5, respectively. Strain sweep experiments shown in **Fig. S5a, b** indicated that both N20 and NH5 samples exhibited a single-step yielding behaviour in both entropic and jammed glass regimes.

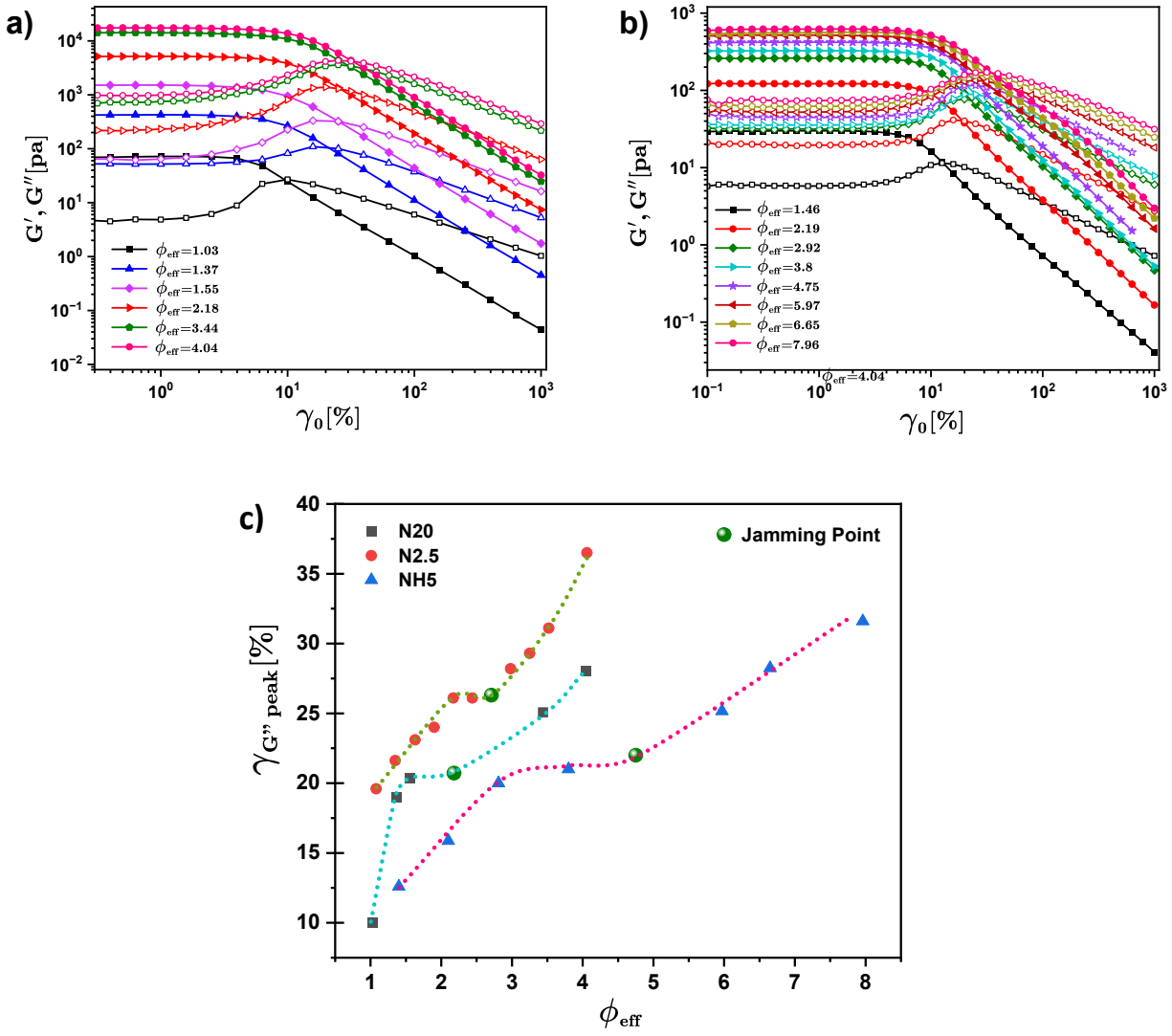

Fig. S5. Dynamic strain sweep experiments for a) N20 microgel and b) NH5 microgel; closed (open) symbols denote G'(G"). c) Strain at which G'' attains its maximum ($\gamma_{G'' Peak}$) versus effective volume fraction.

At higher strain amplitudes, all concentrations consistently display a monotonic decrease of both G' and G'', following a power-law dependence on strain amplitude represented as $G'(\gamma_0) = {\gamma_0}^{-\mu}$ and

$G"(\gamma_0) = \gamma_0^{-\nu}$. Values of μ, and ν obtained by fitting the $G'(\gamma_0) = \gamma_0^{-\mu}$ and $G"(\gamma_0) = \gamma_0^{-\nu}$ for N2.5 microgels are tabulated in Table. S3

Table S4. Parameters extracted from strain sweep measurements conducted in the entropic regime for N2.5 microgels at $\omega = 1\, rad/s$

ϕ_{eff}	μ	ν	m	$G' = G"$ $[Pa]$
1.08	1.38	0.72	0.25	16.25
1.35	1.38	0.72	0.25	18.70
1.62	1.38	0.71	0.26	22.23
1.90	1.36	0.68	0.27	23.39
2.44	1.34	0.65	0.29	25.11
2.71	1.33	0.54	0.30	28.70

VIII. Creep Recovery experiments

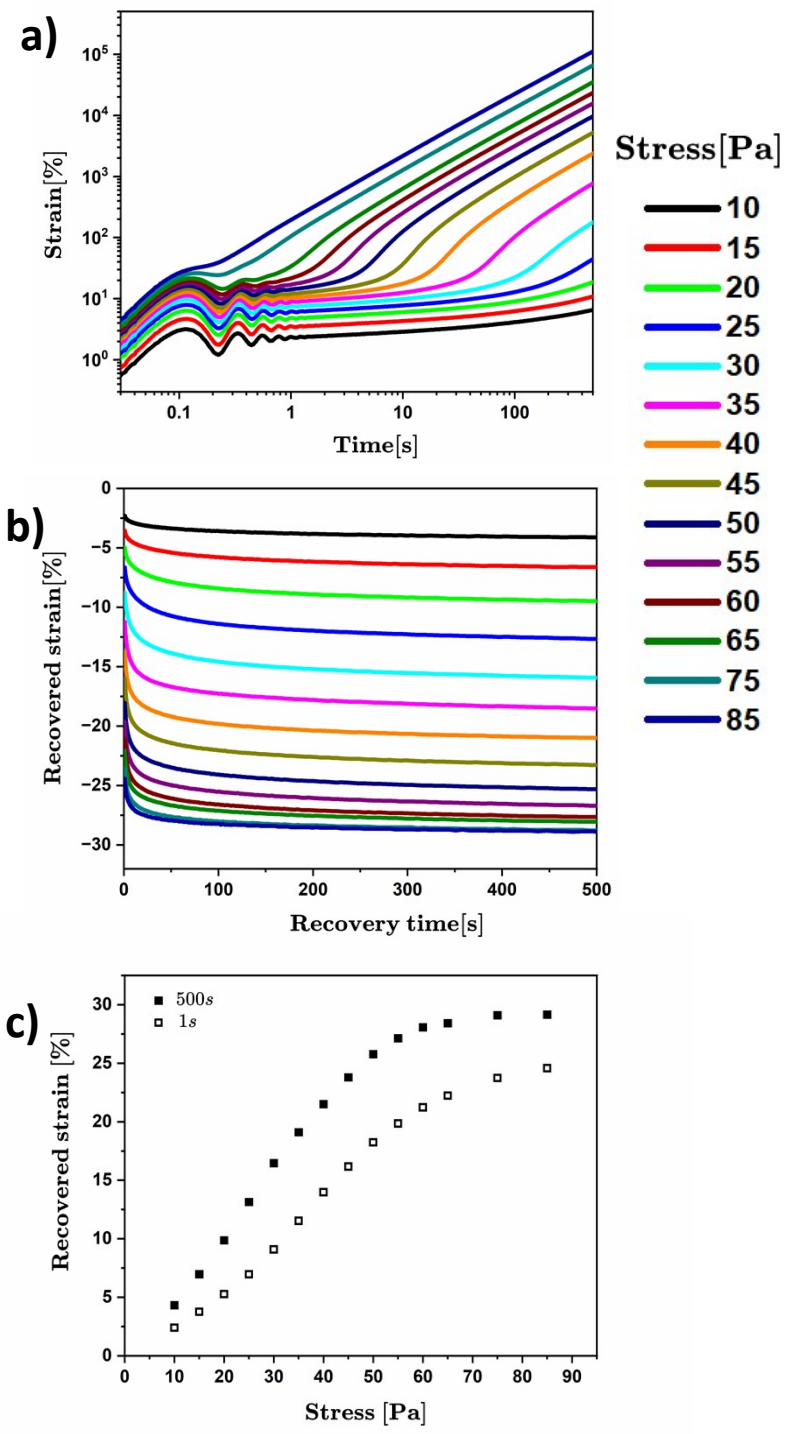

Fig. S6. Creep and recovery experiments for N2.5 particles at $\phi_{eff} = 2.17$: (a) corresponds to creep experiments (b) shows recovered strain as a function of recovery, (c) shows recovered strain (after 1s and 500s) for various applies stress.

IX. Lissajous-Bowditch curves

Fig. S7 shows Lissajous–Bowditch (L-B) curves for various samples. Strain amplitude (γ_0) up to 10% belongs to linear viscoelastic (LVE) region, where L-B curves characterised by a narrow elliptical shape. Between $\gamma_0 = 12.6 - 15.8\%$ strain, we observe the beginning of nonlinearity, indicated by the distorted elliptical shape in the L-B curves, which is a common feature of a strain-softening process[6]. In **Fig S7**, it becomes evident that the strain softening is more pronounced in the entropic glass regime, which are characterized by a greater distortion of the elliptical shape when compared to the jammed glass regime.

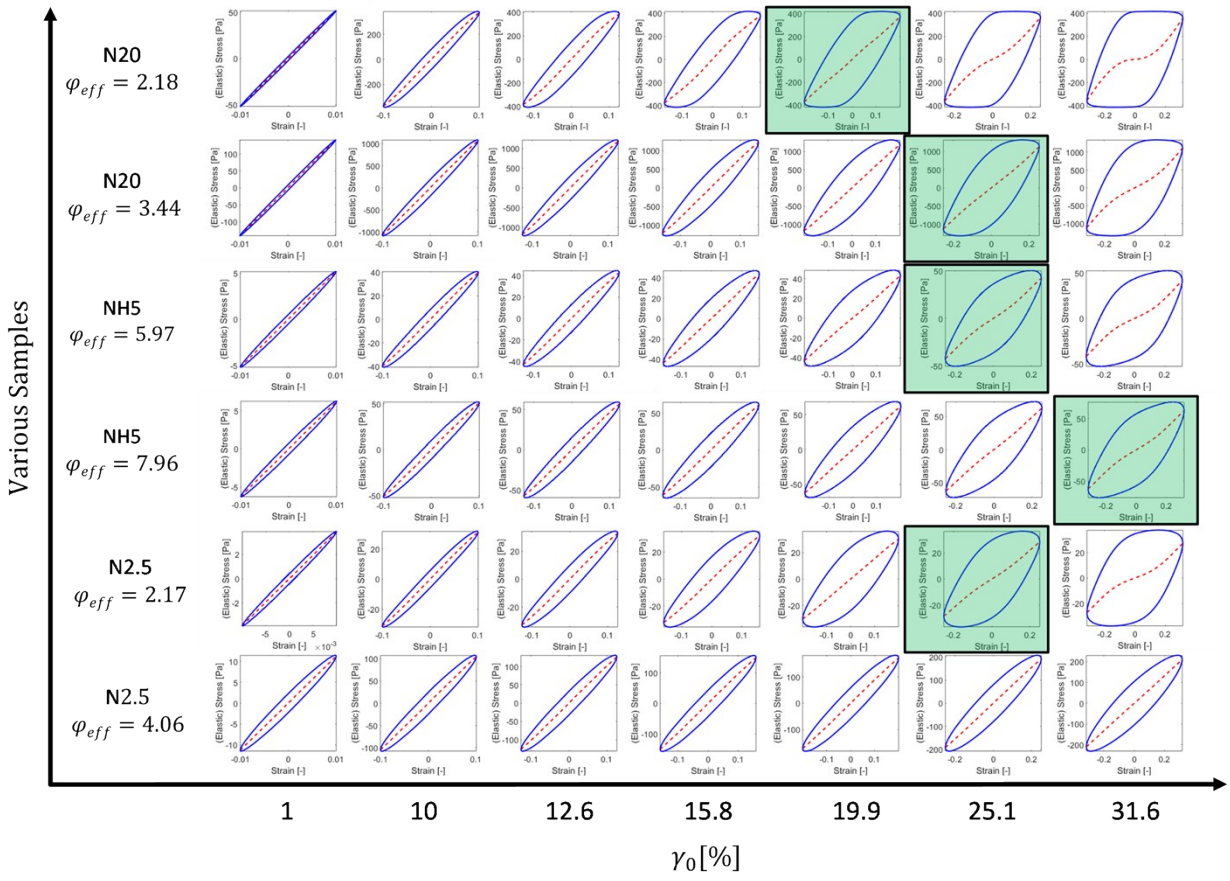

Fig. S7: Stress ($\sigma(t)$)–strain($\gamma(t)$) Lissajous–Bowditch curves for various samples. Sample identities are indicated by the abbreviations on the left side of each row along the vertical axis. Horizontal axis represents strain amplitudes (γ_0). Elastic contributions, extracted via MITlaos, are shown as red dash-dotted lines. Curves corresponding to the first G" peak are highlighted in light green colour.

Notably, L-B curves for jammed glassy regime of N2.5 particle maintain their symmetrical shape at $\gamma_0 = 15.8\%$ and beyond. The G" peak emerges between strain amplitudes of $\gamma_0 = 19.9 - 31.6\%$ across the other samples, signifying the yielding point at which $G" = G'$; all corresponding L-B curves are indicated in **Fig. S7** with light green shading. At this stage, the L-B curve for N20 and NH5 particles in both entropic and jammed glass systems regains its symmetrical shape. The parallelogram shape of L-B curves above this range ($\gamma_0 = 19.9 - 36.1\%$), is an indicative of macroscopic flow. However, for N2.5 particles, a strain-softening effect is evident in the entropic glass regime. In the jammed glassy regime, the L–B curves retain their symmetrical shape even beyond the first G" peak, suggesting that the system continues to exhibit elastic behaviour after the first yielding point. Nevertheless, a gradual increase in the minor axis with increasing strain amplitude is observed.

Fig. S8 shows the evolution of L-B curves with increase in strain amplitude for N2.5 particles at $\phi_{eff} = 4.06$. The first localized yielding event is happening at $\gamma_0 = 39.8\%$, which corresponds to the appearance of the first G'' peak (indicated by light green shade). The elliptical shape in this case retains its symmetry after the first yield point but exhibits an elongated minor axis, indicative of an increased contribution from the viscous component. The elliptical configuration beyond the first yielding point indicate that macroscopic yielding does not occur at the first yield point for N2.5 particles at $\phi_{eff} = 4.06$. Starting at $\gamma_0 = 50.1\%$, the L-B curves exhibit a distorted elliptical shape, with the degree of distortion increasing as the strain amplitude is raised (indicated by light pink shade). This distortion is a typical characteristic of a strain-stiffening process[6]. The maximum strain stiffening is observed just before the second yield point, i.e. at $\gamma_0 = 398\ \%$ strain amplitude. Following the crossover point ($\gamma_0 = 398\ \%$) we observe an ellipse returning to approximately symmetrical form, but with significantly elongated minor axis.

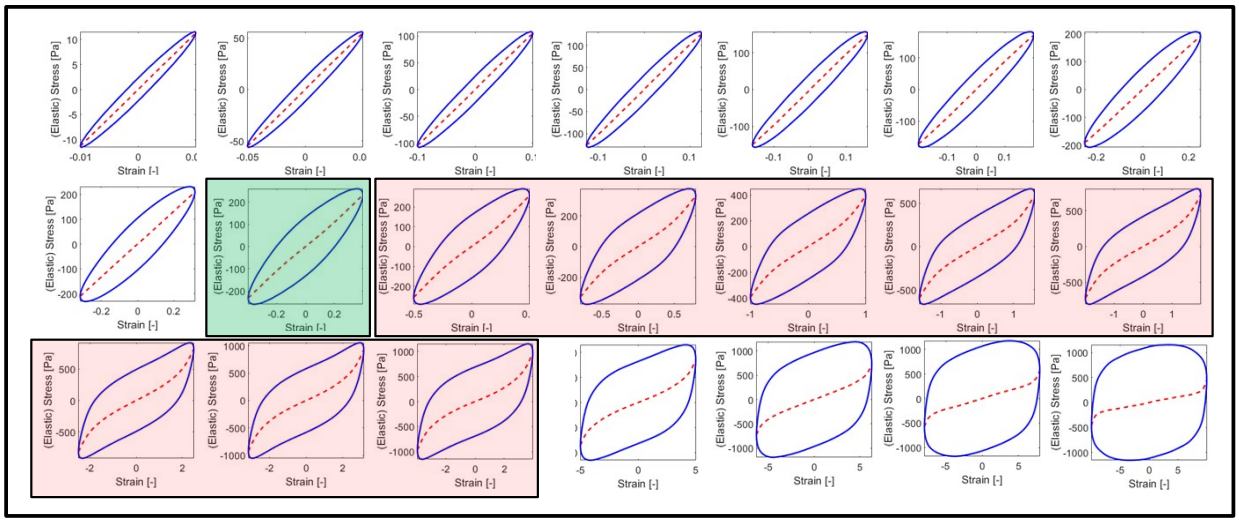

Fig. S8: Shows the evolution of L-B curves of stress, $\sigma(t)$, versus strain, $\gamma(t)$, with increase in strain amplitude for N2.5 particles at $\phi_{eff} = 4.06$ (strain amplitude (%): 1, 5, 10, 12.6, 15.8, 19.9, 25.1, 31.6, 39.8, 50.1, 79.8, 100, 158, 199, 251, 316, 398, 501, 630, 798, and 1000) in an incremental order from left to right and top to bottom. $\gamma_0 = 39.8$ curve is highlighted (light green) to indicate the G" peak, curves between $\gamma_0 = 50.1\%$ and $\gamma_0 = 398\%$ are highlighted (light pink shade) to show the gradual distortion in shape symmetry.

X. Stiffening factor

The strain stiffening ratio, S, and e_3/e_1 obtained are plotted against strain amplitudes for entropic glass regime in **Fig. S9**. Figure shows that the most pronounced strain-softening occurring at $\gamma_0 = 15\%$. N20 particles exhibit comparatively higher stiffening ratio $(S = 20\%)$ when compared to N2.5 and NH5 particles $(S \approx 10\%)$.

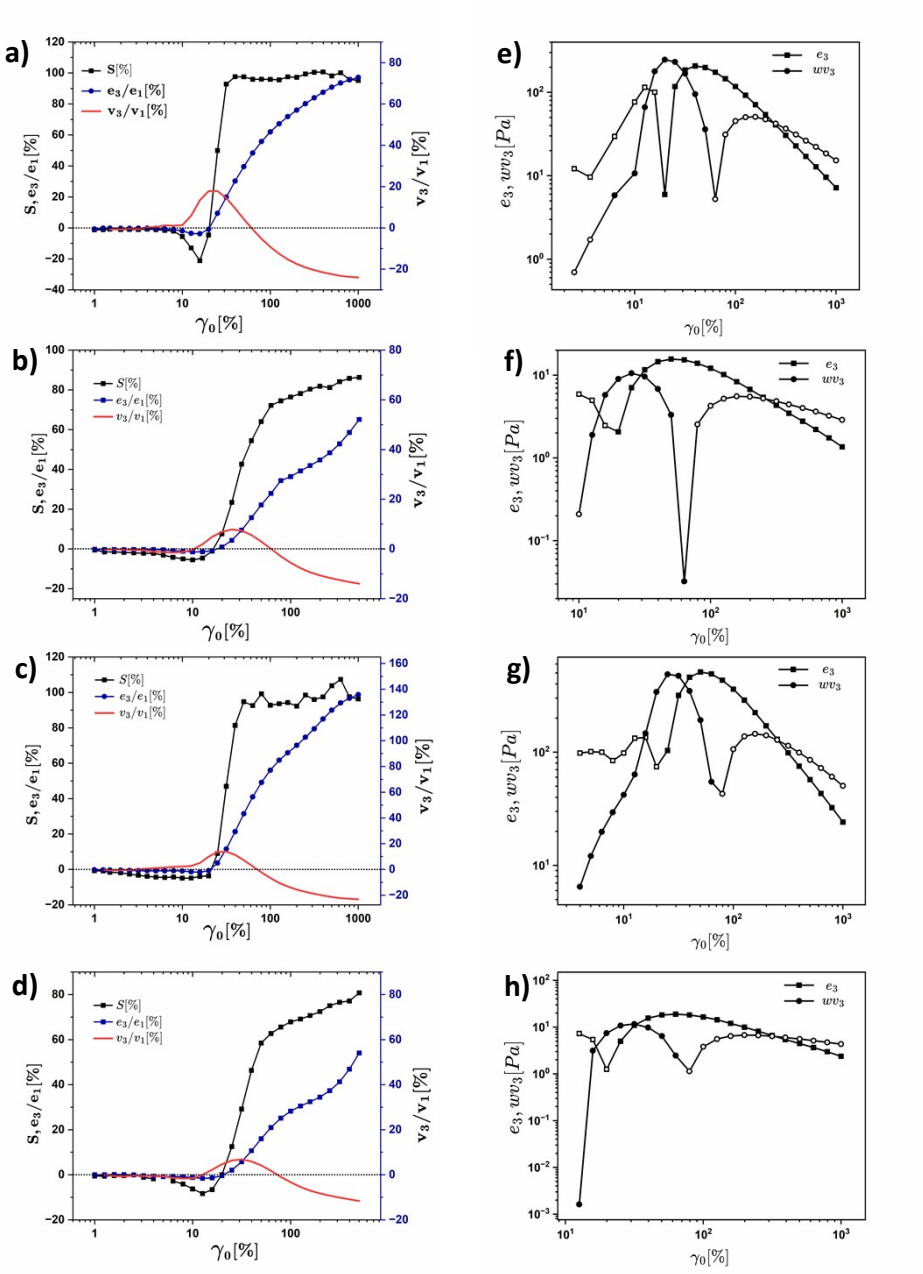

Fig. S9. The strain stiffening ratio, S, e_3/e_1, and v_3/v_1 are plotted against strain amplitudes: (a) N20 at $\phi_{eff} = 2.18$, (b) NH5 at $\phi_{eff} = 5.97$, (c) N20 at $\phi_{eff} = 3$.44 (d) NH at $\phi_{eff} = 7.96$. Absolute values of e_3 (square) and ωv_3 (round) are shown in (e, f, g, h) as the functions of the strain amplitudes for (e) N20 at $\phi_{eff} = 2.18$, (f) NH5 at $\phi_{eff} = 5.97$, (g) N20 at $\phi_{eff} = 3$.44 (h) NH at $\phi_{eff} = 7.96$ (open symbols used when e_3 and ωv_3 are negative)

References

1 R. Acciaro, T. Gilányi and I. Varga, *Langmuir*, 2011, **27**, 7917–7925.
2 A. Ikeda, L. Berthier and P. Sollich, *Phys. Rev. Lett.*, 2012, **109**, 018301.

3 T. Mason, M.-D. Lacasse, G. Grest, D. Levine, J. Bibette and D. Weitz, *Phys. Rev. E*, 1997, **56**, 3150–3166.
4 G. Chaudhary, A. Ghosh, J. G. Kang, P. V. Braun, R. H. Ewoldt and K. S. Schweizer, *J. Colloid Interface Sci.*, 2021, **601**, 886–898.
5 M. A. Lara-Peña, A. Licea-Claverie, I. Zapata-González and M. Laurati, *J. Colloid Interface Sci.*, 2021, **587**, 437–445.
6 R. H. Ewoldt, A. E. Hosoi and G. H. McKinley, *J. Rheol.*, 2008, **52**, 1427–1458.